AIAA JOURNAL
Vol. 42, No. 5, May 2004

Evaluation of a Multi-Axial, Temperature- and Time-Dependent Failure Model

D. E. Richardson,* G. L. Anderson,† and D. J. Macon‡
ATK Aerospace Company, Brigham City, Utah 84302-0707

To obtain a better understanding of the response of the structural adhesives used in the space shuttle's reusable solid rocket motor (RSRM) nozzle, an extensive effort has been conducted to characterize in detail the failure properties of these adhesives. This effort involved the development of a failure model that includes the effects of multi-axial loading, temperature, and time. An understanding of the effects of these parameters on adhesive failure is crucial to the prediction of safety of the RSRM nozzle. The use of this newly developed multi-axial, temperature, and time-dependent failure model for modeling failure for the adhesives TIGA 321, EA913NA, and EA946 is documented. The development of the mathematical failure model using constant load rate data for both normal and shear loading is presented. Verification of the accuracy of the failure model is shown through comparisons between predictions and measured creep and multi-axial failure data. The verification indicates that the failure model performs well for a wide range of conditions (loading, temperature, and time) for the three adhesives. The failure criterion is shown to be accurate through the glass transition for the EA946 adhesive. Though this failure model has been developed and evaluated with adhesives, the concepts should be applicable for other isotropic materials.

Introduction

BECAUSE of industrial safety and obsolescence issues, several adhesives (EA913NA and EA946) used in the space shuttle's reusable solid rocket motor (RSRM) nozzle (Fig. 1) are being replaced with an improved adhesive (TIGA 321). To ensure the safety and integrity of this TIGA 321 adhesive for use in a human-rated system, a thorough material characterization test program has been completed. This characterization was conducted on both the current adhesives and the replacement adhesive so that accurate comparisons could be made. Part of this study involved the evaluation of the effects of multi-axial loading, temperature, and time on failure behavior. Traditionally, the effects of each of these conditions are accounted for separately. This paper documents the development and verification of a combined multi-axial, temperature-, and time-(MATT-) dependent failure criterion for the three aforementioned adhesives. The criterion was developed with TIGA 321 (Ref. 1), EA913NA and EA946 to evaluate its applicability to multiple adhesive systems.

MATT

The MATT-dependent failure criterion developed by the authors is a combination of several accepted failure criteria (to be discussed) of the following form:

$$AP^2J_2 + BPI_1 = 1 \tag{1}$$

J_2 is the second deviatoric stress invariant, and I_1 is the first stress invariant. These invariants can be shown to be of the following form for an arbitrary stress state:

$$J_2 = \frac{1}{3}\begin{bmatrix} \sigma_{11}^2 + \sigma_{22}^2 + \sigma_{33}^2 \\ -\sigma_{11}\sigma_{22} - \sigma_{11}\sigma_{33} - \sigma_{22}\sigma_{33} \\ +3\sigma_{12}^2 + 3\sigma_{13}^2 + 3\sigma_{23}^2 \end{bmatrix}$$

$$I_1 = \sigma_{11} + \sigma_{22} + \sigma_{33} \tag{2}$$

A and B are parameters that define the shape of the failure envelope (which is ellipsoidal in nature). As will be shown, the A and B parameters (hence, the ellipsoidal shape of the failure curve) are independent of time and temperature. The P parameter is the factor that is used to scale the size of the failure envelope to account for temperature and time effects.

This failure model is equivalent to a form of the Tsai–Wu[2] criterion and a modified Drucker–Prager criterion[3] if P is held constant. The P scaling factor extends the utility of this form of the Tsai–Wu and Drucker–Prager criteria by accounting for the effects of temperature and time.

Linear Cumulative Damage

For this paper, the P factor is modeled using a linear cumulative damage technique.[4–6] This cumulative damage model will focus on a series of time- and temperature-dependent constant load rate tests. When the MATT equation is used, this time- and temperature-dependent failure model will be expanded to account for general (multi-axial) loading conditions.

The form of the linear cumulative failure model used in this paper is as follows:

$$N_\sigma = \left[\int_0^{t_f} \sigma_i^\beta \, \mathrm{d}t\right]^{1/\beta} \tag{3}$$

N_σ and β are failure coefficients (which are a function of temperature), and σ_i is the applied stress as a function of time. Failure occurs at a stress level σ_f and a failure time t_f.

For this study, constant load rate test data were used to characterize the time and temperature dependence of the P scaling factor. As will be discussed, other test data (resulting from constant load/creep conditions) are used for verification of the failure model.

To account for the time (rate) and temperature effects, the linear cumulative damage equation can be simplified for the following basic loading conditions.

For constant loading rate conditions,

$$t_f = (1+\beta)[N_\sigma/\sigma_f]^\beta, \qquad \sigma_f = N_\sigma[t_f/(1+\beta)]^{-1/\beta} \tag{4}$$

For constant stress (or creep) loading conditions,

$$t_f = (N_\sigma/\sigma_f)^\beta, \qquad \sigma_f = N_\sigma t_f^{-1/\beta} \tag{5}$$

Received 8 June 2002; revision received 7 February 2003; accepted for publication 7 February 2003.

*Structural Analyst, ATK Thiokol Propulsion Division.
†Material Scientist, ATK Thiokol Propulsion Division.
‡Polymer Engineer, ATK Thiokol Propulsion Division.

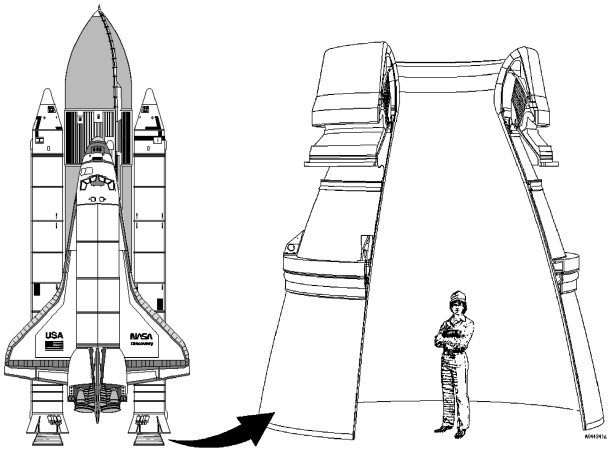

Fig. 1 Space shuttle RSRM nozzle.

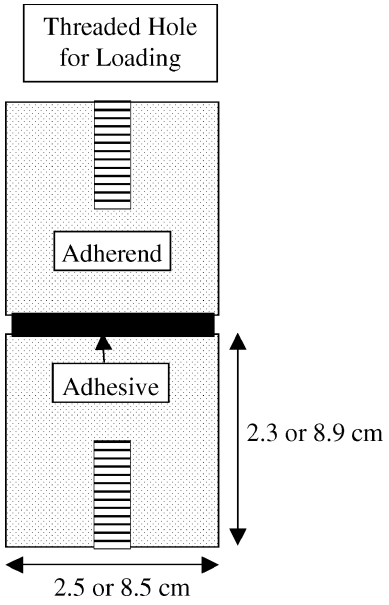

Fig. 2 Tensile adhesion button.

Test Specimen Preparation

For all of the testing described in this paper, all of the adherends were manufactured of steel or aluminum. The bond surfaces were prepared by aqueous alkaline detergent cleaning, grit blasting, and priming (silane based).

The adhesives used in this study are commercially available aromatic and aliphatic amine-cured epoxies. Fiber and/or powder fillers are used in the formulations. The adhesives were vacuum mixed. Standard cure cycles developed for the space shuttle's RSRM nozzle processing were used for the adhesives. All specimens were conditioned under ambient conditions for at least 3 days before testing. The glass transition temperature for EA946 is approximately room temperature. The glass transition temperature for EA913NA and TIGA 321 is greater than 50°C.

Temperature and Time Testing

The P scaling factor can be modeled by characterizing the temperature and time dependence of the adhesive for a consistent stress configuration, for example, pure normal, pure shear, or consistent multi-axial. For this study, the temperature and time dependence was characterized using tensile adhesion tests. These tensile adhesion tests were conducted using a universal tensile testing machine with temperature conditioning chambers. Loads, displacements, and time were digitally recorded during each test. Specimens of different diameters ranging from 2.5 to 8.5 cm were used depending on the adhesive. The basic test specimen geometry is shown in Fig. 2. The larger specimens were used for the EA946 adhesive, the smaller specimens were used for EA913NA and TIGA 321. Bondline aspect ratios ranged from approximately 10 to over 100. Low bondline aspect ratio specimens (specimens with thick bondlines) were tested so that adhesive strain measurements could be made for another investigation. For this study, only the ultimate stress measurements were used (for all bondline aspect ratios). All material characterization testing was conducted with a single specimen geometry. The verification testing in some cases was conducted with specimens of a different geometry. (The verification specimens were consistent for a given adhesive.)

Because of this variation in test specimens, the triaxial bondline stress state of each individual specimen was taken into account for the evaluation. The triaxial stress state is caused by the rigid adherends that restrict Poisson's contractions of the adhesive during loading. It was assumed that the effects of thermal expansion/contraction were negligible on the stress state being evaluated. It was also assumed that the stress concentration factor calculated for each specimen for room temperature test conditions (20°C) was constant for all temperatures.

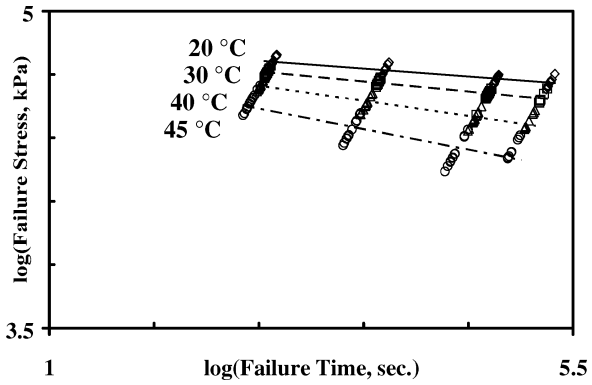

Fig. 3 TIGA-321 tensile button failure data.

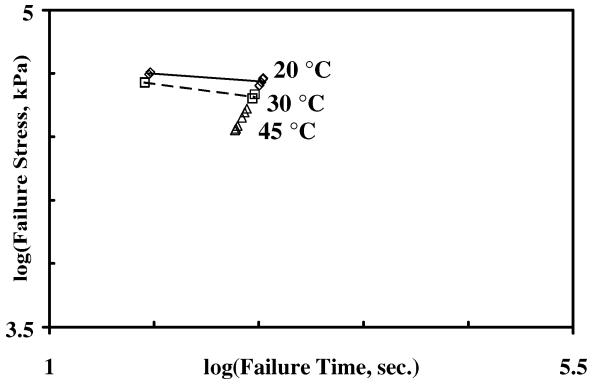

Fig. 4 EA913NA tensile button failure data.

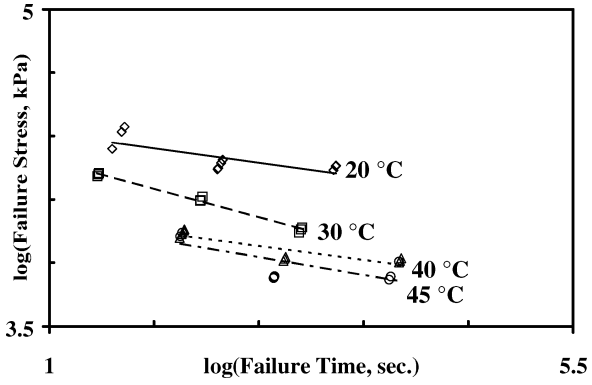

Fig. 5 EA946 tensile button failure data.

To generate the failure model, tests were conducted at temperatures ranging from −10 to 45°C and at three or four load rates (depending on the adhesive) that had failure times ranging from approximately 1 min to 3 days. The load rates differed by an order of magnitude. In general, TIGA and EA913NA failure modes were cohesive in the adhesive. EA946 failure modes were approximately 50% interfacial and 50% cohesive in the adhesive. (Typically, there was more interfacial failure for higher temperatures and longer times.) The temperature- and time-dependent nature of the adhesives was characterized through the data from this testing. It was found that there was very little time dependence in failure for these adhesive for temperatures at or below 5°C (well below the glass transition temperature for the three adhesives).

The test data that were used to generate the cumulative damage failure coefficients N_σ and β are shown in Figs. 3–5. Least-square line fits of the data points are shown in the curves. Similar data were obtained at −10 and 5°C, which are not included in Figs. 3–5. For these temperatures, the line connecting the failure data was nearly horizontal, indicating little or no time dependence. As can be seen in the Fig. 4, the amount of characterization data for the EA913NA adhesive was limited in number. The characterization data for EA946 was very scattered and limited in number (Fig. 5). The variation is attributed to testing at temperatures near the glass transition temperature of EA946. (EA946 has a wide glass transition range.) As will be seen later, even with these limitations for EA913NA and EA946, accurate predictions of failure are made.

The test temperatures are below the glass transition temperature for TIGA 321 and EA913NA. For both adhesives, the glass transition temperature is greater than 50°C. The test temperatures bound the glass transition temperature for EA946, which is approximately room temperature (20°C). This EA946 adhesive provides a good evaluation of the validity of the failure model through and above the glass transition.

To address the temperature effects on failure, the N_σ and β values (which define the time-dependent nature of failure) for each adhesive and each temperature were obtained using Eqs. (4) and the data are seen in Figs. 3–5. N_σ and β were not determined for temperatures at or below 5°C. N_σ and β were found to vary linearly with temperature for test data ranging from 20 to 45°C:

$$N_\sigma = m_N T + b_N, \qquad \beta = m_\beta T + b_\beta \tag{6}$$

If these linear relationships derived from Figs. 3–5 are input into the cumulative damage failure model, a single temperature- and time-dependent failure model is developed for the regime of time dependence (from 20 to 45°C). This model is then combined with the time-independent nature of failure at temperatures below 5°C, and the temperature- and time-dependent nature of the adhesive is fully characterized for the range of interest.

This failure characterization, however, is restricted to the tensile adhesion button loading. In the following sections, this relationship will be expanded using the MATT equation to account for multi-axial loading.

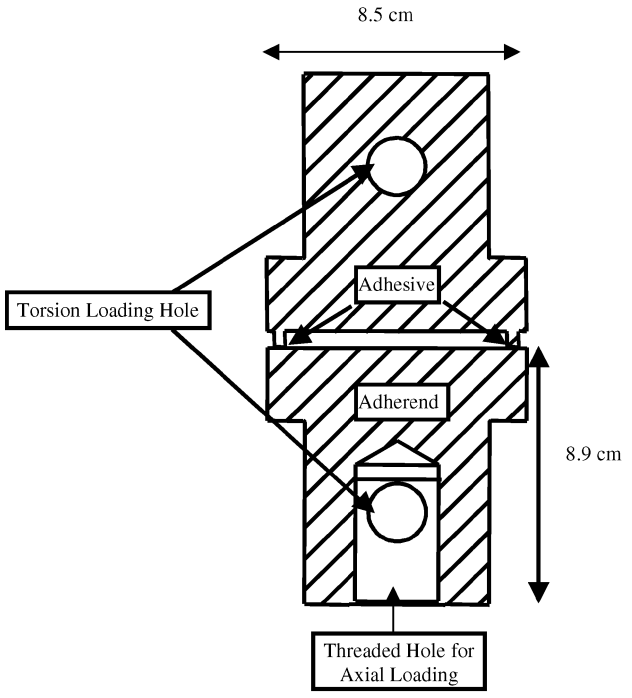

Fig. 6 Napkin ring test specimen.

Multi-Axial Characterization

To characterize the multi-axial nature of failure, the time and temperature dependence of shear failure was also evaluated. These shear adhesion tests were conducted using an axial/torsion testing machine with a temperature conditioning chamber. Loads, displacements, and time were digitally recorded during each test. Testing was conducted using napkin ring shear adhesion specimens[7,8] (also

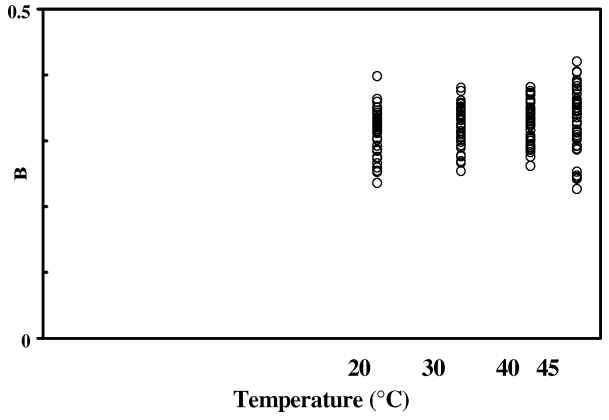

Fig. 7 *B* vs temperature for TIGA 321.

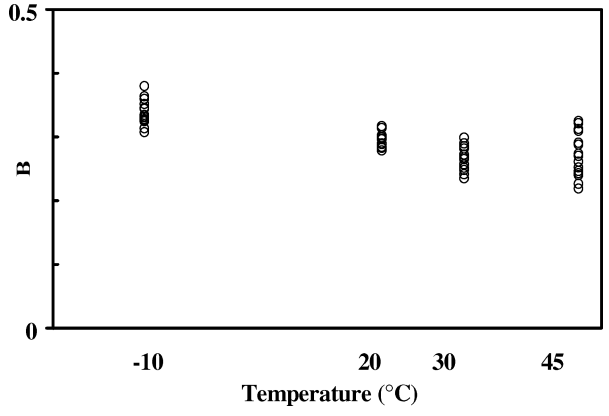

Fig. 8 *B* vs temperature for EA913NA.

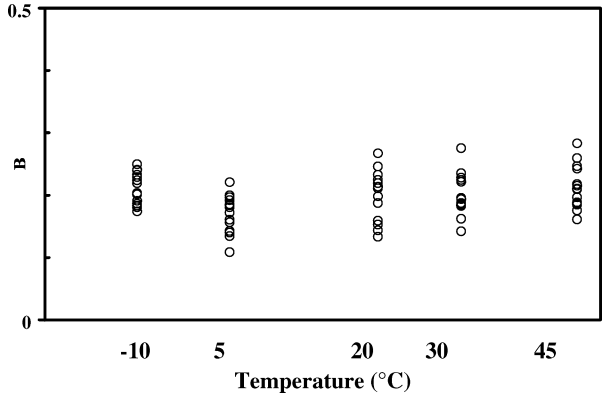

Fig. 9 *B* vs temperature for EA946.

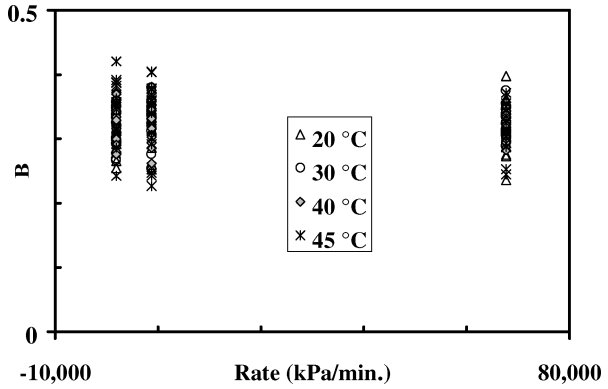

Fig. 10 *B* vs load rate for TIGA 321.

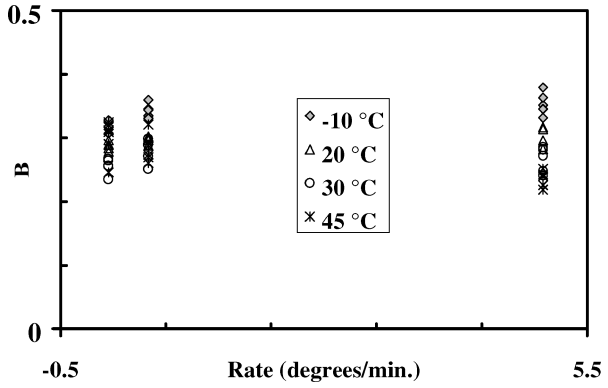

Fig. 11 *B* vs load rate for EA913.

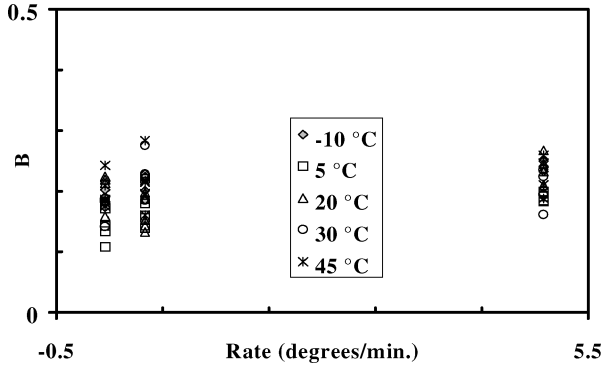

Fig. 12 *B* vs load rate for EA946.

Anderson, G. L., Crook, R. A., Richardson, D. E., and Boothe, oral presentation at Summer Meeting of the American Society of Mechanical Engineers, 1991) (Fig. 6). The diameter was approximately 8.5 cm for all testing.

Shear adhesion tests were also conducted at temperatures ranging from −10 to 45°C with load rates that had failure times ranging from approximately 20 s to 1 h. The load rates differed by an order of magnitude.

The multi-axial nature of failure of the three adhesives was mathematically evaluated by making predictions of average tensile adhesion button failure loads (using the linear cumulative damage failure model described earlier) at temperatures and failure times equivalent to those of the shear adhesion tests. For each shear adhesion test data point, and its accompanying predicted tensile adhesion button failure load, values for A, B, and P of the MATT equation were calculated. These MATT parameters mathematically defined the failure ellipsoid that describes the multi-axial failure for the given

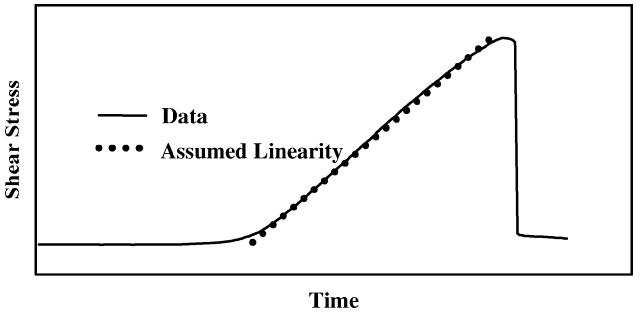

Fig. 13 Example of shear test conducted under constant twist angle control.

time and temperature conditions of the test specimen. (The ellipsoid passes through the shear and tensile failure values.) In these assessments, the tri-axial nature of the stress state in the tensile adhesion specimens was taken into account.

Because the A and B parameters are assumed to define the shape of the failure ellipsoid independent of temperature and time, the A parameter was assumed to be 1.0. The calculated B parameter defined the shape of the ellipsoid, and the calculated P parameter defined the size of the ellipsoid. The B factor as a function of temperature for each of the three adhesives can be seen in Figs. 7–9.

As can be seen in Figs. 7–9, the B factor does not appear to be dependent on temperature for the three adhesives. Of particular interest are the data for EA946, where the test data bridge the glass transition for the adhesive (approximately 20°C). If the shape factors A and B were dependent on temperature, it would be expected to show up for EA946. The source of scatter in the data is unknown; however, note that the amount of scatter for EA946 (which is highly temperature dependent) is comparable to that of TIGA 321 (which is not as temperature dependent).

B as a function of torsional loading rate is shown in Figs. 10–12. Note that the TIGA 321 adhesive shear adhesion specimens were loaded in a constant shear stress rate. (A constant torsional load rate was applied to the specimen.) For the adhesives EA913NA and EA946, the specimens were loaded in constant twist angle rate control (not constant load rate). For this loading condition, the load rate was nearly constant (except at the beginning of loading). To make the calculations for this study, it was assumed that the load rate was constant. The failure time was back calculated using the linear region of the load time curves. (See Fig. 13 for an example.) As can be seen in the Figs. 10–12, there does not appear to be a time dependence on the A and B factors when all of the data are considered together.

A study of the change in B as a function of load rate for each individual temperature indicates a slight tendency for B to increase with load rate for some temperatures. This, however, is not a general trend. (For a limited number of temperatures, the trend is opposite.) Therefore, it is unclear whether this trend is actual or due to scatter in the test data. For this study, B is assumed to be constant. As will be seen later, the predictions are good using this assumption.

Failure Criterion

The MATT failure criterion is assembled by combining the findings from the linear cumulative damage failure model and the multi-axial testing described earlier. This can be completed through mathematical relationships or numerically. Because of the complex nature of the triaxial loading in the tensile adhesion specimens used for this testing, a numerical approach was utilized for this study to define the P parameter.

Table 1 contains predictions of coefficients of variation of all of the tensile adhesion and shear data combined when compared to the MATT failure model for the three adhesives. These statistics indicate a very good fit for test data over a wide range of temperatures and failure times. There is more scatter in the EA946 test data. This is assumed to be due to testing near the glass transition temperature.

Table 1 Failure criterion statistics

Adhesive	Number of specimens	Coefficient of variation, %
TIGA 321	384	9.2
EA913NA	84	10.6
EA946	132	16.7

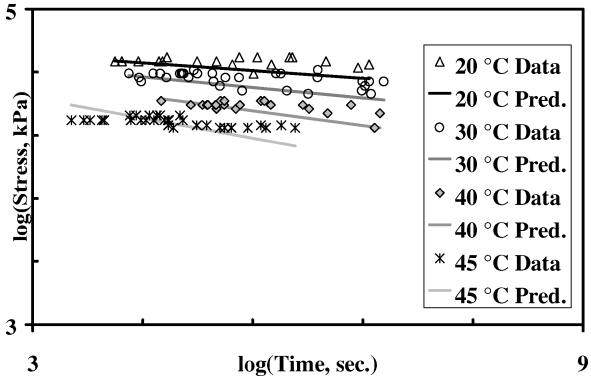

Fig. 14 Creep failure predictions for TIGA 321.

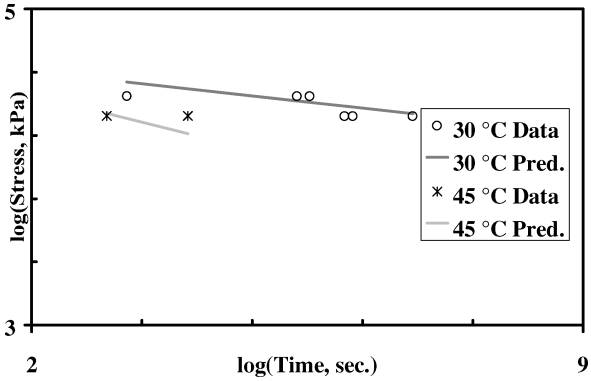

Fig. 15 Creep failure predictions for EA913NA.

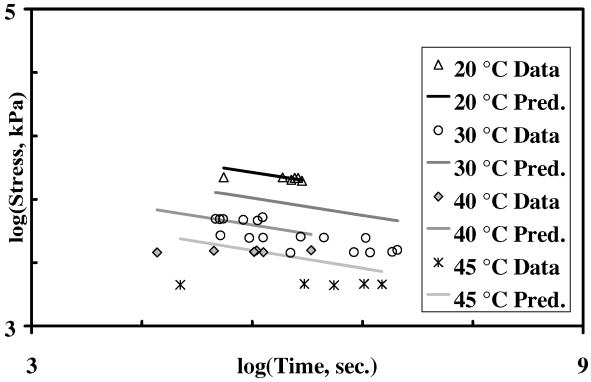

Fig. 16 Creep failure predictions for EA946.

MATT Verification

Verification of the accuracy of the MATT failure criterion was evaluated using both creep failure test data and multi-axial test data. Creep failure was used to evaluate the accuracy of the MATT criterion to predict time and temperature effects. Multi-axial testing was also conducted to evaluate the ability of the MATT criterion to predict the combined multi-axial and temperature effects.

Creep Failure

Creep resistance testing was conducted using tensile adhesion specimens as described earlier. These creep tests were conducted using a creep tensile facility with temperature conditioning chambers. Loads, displacements, and time were digitally recorded during tests. Loads were applied such that failure times ranged from less than 1 h to approximately 5 months. This testing provided an evaluation of the MATT criterion under a unique loading condition (different from that used to generate the model) and at extended failure times (much greater than those used to generate the failure model).

There was significant scatter associated with this type of testing. As will be shown later, the combined statistics for all of the testing are good even with this scatter.

MATT predictions of creep failure can be seen in Figs. 14–16. In general, TIGA and EA913NA failure modes were cohesive in the adhesive. EA946 failure modes were approximately 50% interfacial and 50% cohesive in the adhesive. (Typically there was more interfacial failure for higher temperatures and longer times.) To allow for the evaluation of the criterion in the exponential regime of the linear cumulative damage model, the data are plotted on log–log axes. As can be seen in Figs. 14–16, the model provides good failure predictions for TIGA 321 and EA913NA. The prediction for EA946 is fair.

A study was conducted to evaluate the variation of the EA946 data from prediction. It was found that the scatter noted in the test data shown in Fig. 5 caused this variation from prediction. Removal of some questionable data points would give a better fit. However, the authors elected to include all data points for this paper. This scatter is attributed to testing being conducted near the glass transition temperature with weak controls on the test temperature. For EA946, small variations in temperature (near the glass transition temperature) cause significant variations in material properties. Even with the effects of scatter, the predictions are adequate to make good estimates of failure. A statistical A-basis prediction (99% probability and 95% confidence) bounds the EA946 data (with a few expected outliers).

The test data indicate the characterization of the time and temperature dependence of the three adhesives was successful over this wide range of times and temperatures.

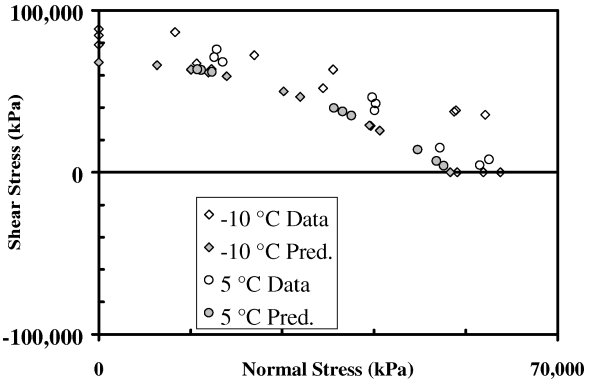

Fig. 17 Multi-axial predictions and data for TIGA 321.

Multi-Axial Failure

As already mentioned, the multi-axial nature of the MATT failure theory was evaluated using test data generated with the napkin ring specimen[7,8] (also oral presentation cited earlier) on the axial/torsion test machine. For these tests, the specimens were loaded with a combination of both normal and shear stresses. The raw test data and the MATT prediction can be seen in Figs. 17–22. As can be seen, the predictions accurately match the test data. Of particular interest are the data for EA946 where the predictions are good through the glass transition temperature regime.

Statistical Evaluation

All of the test data (original and verification) were combined to evaluate the overall accuracy of the MATT failure model. The predicted coefficient of variation of the data from the prediction can be seen in Table 2. The coefficients of variation of the test data are very good given the extreme range of temperatures, failure times, and multi-axial loading conditions. Even for EA946, the predictions have a good accuracy considering the proximity of the testing to the glass transition.

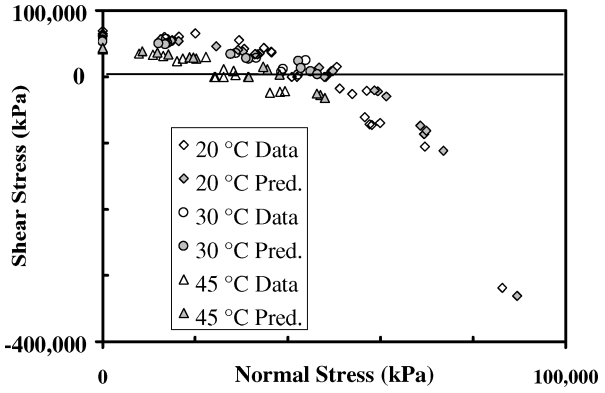

Fig. 18 Multi-axial predictions and data for TIGA 321.

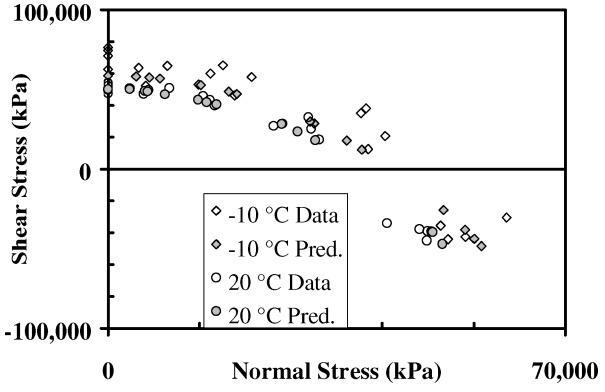

Fig. 19 Multi-axial predictions and data for EA913NA.

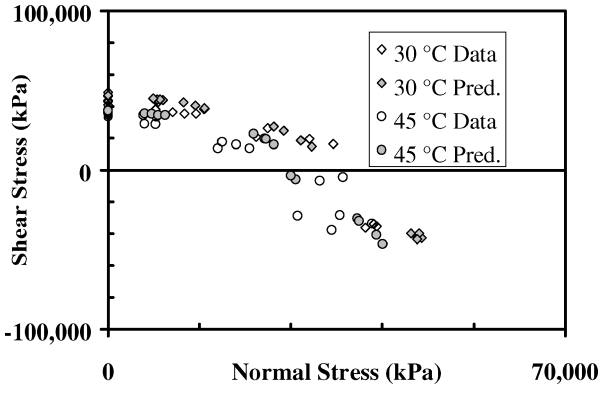

Fig. 20 Multi-axial predictions and data for EA913NA.

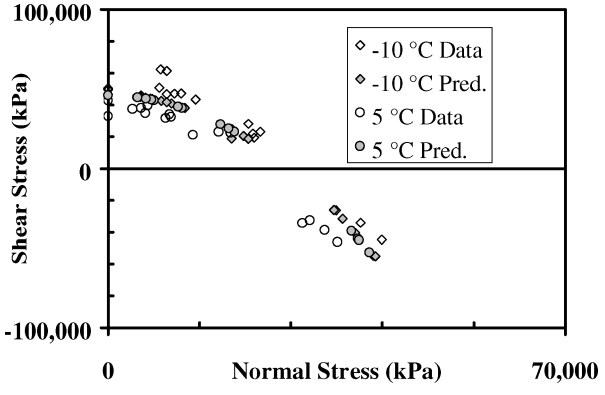

Fig. 21 Multi-axial predictions and data for EA946.

Table 2 MATT statistics

Adhesive	Number of specimens	Coefficient of variation, %
TIGA 321	568	11.3
EA913NA	168	12.1
EA946	240	20.0

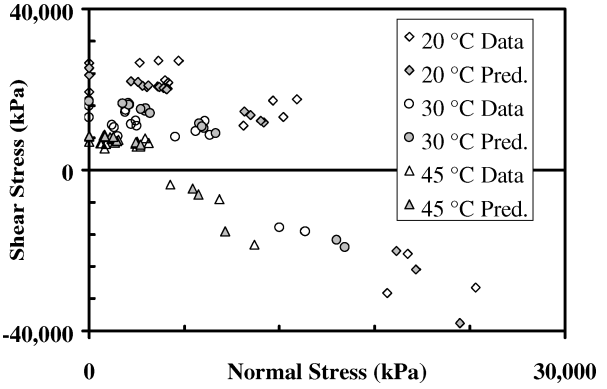

Fig. 22 Multi-axial predictions and data for EA946.

Conclusions

The MATT failure criterion has been evaluated for three adhesives. The failure criterion has been shown to be applicable for temperatures ranging from −10 to 45°C and has been shown to predict tensile failure accurately for both constant load rate and constant load test specimens with failure times ranging from minutes to months. The criterion has also been shown to be accurate for a wide range of multi-axial loading conditions. Of particular interest is the accuracy of the model for the adhesive EA946 when evaluated near the glass transition regime. It is recommended that additional tests near and above the glass transition temperature be conducted to provide additional verification of the model. The failure criterion is general and should be possible to extend to other material systems.

The test data indicate that the shape of the failure ellipsoid, as defined by the A and B parameters, can be assumed to be independent of temperature and failure time. The data also indicate that the size of the failure ellipsoid, modeled with the P parameter, varies with temperature and time.

References

[1]Richardson, D. E., McLennan, M. L., Anderson, G. L., Macon, D. J., and Batista-Rodriguez, A., "Multi-Axial, Temperature and Time Dependent (MATT) Failure Model," *Proceedings of the 25th Annual Meeting of the Adhesion Society and WCARP-II*, Adhesion Society, Blacksburg, VA, 2002, pp. 68–70.

[2]Tsai, S. W., and Wu, E. M., "General Theory of Strength for Anisotropic Materials," *Journal of Composite Materials*, Vol. 5, 1971, pp. 58–63.

[3]Drucker, D. C., and Prager, W., "Soil Mechanics and Plastic Analysis or Limit Design," *Quarterly of Applied Mathematics*, Vol. 10, 1952, pp. 157–165.

[4]Laheru, K. L., "Development of a Generalized Failure Criterion for Viscoelastic Materials," *Journal of Propulsion and Power*, Vol. 8, No. 4, 1992, pp. 756–759.

[5]Batista-Rodriguez, A., and Richardson, D. E., "Time/Temperature Dependent Uniaxial and Shear Failure Characterization of an Adhesive," JANNAF RNTS Subcommittee Meeting, CPIA Publ. 707, Chemical Propulsion Information Agency, Columbia, MD, 2001, pp. 171–179.

[6]Richardson, D. E., Batista-Rodriguez, A., and Macon, D. J., "Evaluation of a Linear Cumulative Damage Failure Model for an Epoxy Adhesive," AIAA Paper 2001-3720, 2001.

[7]McCarvill, W. T., and Bell, J. P., "Torsional Test Method for Adhesive Joints," *Journal of Adhesion Science*, Vol. 6, 1974, pp. 185–193.

[8]Bryant, R. W., and Dukes, W. A., "The Measurement of the Shear Strength of Adhesive Joints in Torsion," *British Journal of Applied Physics*, Vol. 16, 1965, pp. 101–108.

K. N. Shivakumar
Associate Editor